

# Combustion Regime Classification of HCCI Combustion using Lagrangian Fluid Particle Tracking

Naoya Fukushima, Makito Katayama, Masayasu Shimura,  
Mamoru Tanahashi, Toshio Miyauchi

Department of Mechanical and Aerospace Engineering, Tokyo Institute of Technology  
2-12-1 Ookayama, Meguro-ku, Tokyo 152-8550, Japan

## 1 Introduction

Homogeneous charge compression ignition (HCCI) engine has a potential for higher efficiency compared with spark ignition engine, and for lower emission compared with diesel engine. Therefore, HCCI engine is expected as one of the promising combustion technologies [1]. However, there are a lot of unresolved issues to realize HCCI engine practically. One of the most serious issues is control of ignition. Recently, DNS studies related to HCCI of hydrogen–air and n-heptane–air mixtures have been performed [2–4], and effects of inhomogeneity of mixture fraction and temperature on HCCI combustion have been investigated. For more accurate prediction using Multi-Zone model [5] or flamelet model [6], it is required to clarify effects of heat and species diffusion on autoignition and classify combustion regimes in detail. Ju et al. [7] conducted one dimensional simulation of spark assisted HCCI combustion of n-heptane–air mixture and revealed that there exist at least six different combustion regimes and mentioned that transition of each combustion regime is one of the key for a separated ignition and flame propagation model. The method by Yoo et al. [4] based on chemical explosive mode analysis and Damköhler number can distinguish the combustion regimes between spontaneous ignition and deflagration waves at an instantaneous combustion field, but cannot clarify how much fuel is consumed in what kinds of combustion regime throughout whole combustion process since the method does not consider temporal development.

In the present study, DNS studies of autoignition of methane–air and n-heptane–air mixtures are conducted by considering realistic kinetic mechanism and temperature dependence of transport and thermal properties to investigate influences of spatial inhomogeneity of temperature on turbulent HCCI combustion. By introducing Lagrangian fluid particle tracking to DNS, combustion regime classification method in HCCI combustion is proposed.

## 2 Direct Numerical Simulation of Turbulent HCCI Combustion

In this study, considering actual HCCI combustion, numerical conditions are determined. In most cases, intake temperature and compression ratio conditions range from 300 K to 400 K and 10 to 20, respectively. Intake temperature and compression ratio conditions are set to 400 K and 18:1. Since the HCCI

engines are operated in the lean condition, equivalence ratio is set to 0.3. Furthermore, it is supposed that chemical reaction starts from crank angle of -3 deg. Under the assumption of the adiabatic change without chemical reactions, mean temperature and pressure increase up to 1149.3 K and 51.3 atm for methane–air case and 1137.2 K and 50.5 atm for n-heptane–air case, respectively, from 1.0 atm. These values are used as the initial mean temperature and pressure for DNS for each case.

The geometry of combustion and flow field is a two dimensional square field filled with turbulent pre-mixed mixture. Fully-developed homogeneous turbulence at  $Re_\lambda = 179.0$  is adopted as the initial velocity field and the turbulent intensity ( $u'_{rms}$ ) is set to be 3.69 m/s. Under the condition, the integral length scale of turbulence is 0.364 mm. The mixtures with spatial inhomogeneity of temperature are investigated. Integral length scale of the initial temperature fluctuations is 0.375 mm which is comparable to that of the initial turbulence. Root mean square (RMS) of the initial temperature fluctuations ( $T'_{init}$ ) is set to 12 K, 60 K, 90 K and 120 K for methane–air mixtures and 12 K and 60 K for n-heptane–air mixtures, respectively. It is noted that large and fine scale eddies enhance mixing of temperature and induce small-scale temperature fluctuations in short period at high Reynolds number in real engine, even when only large-scale temperature fluctuations exist initially. The size of the computational domain is  $L_x \times L_y = 1.875 \text{ mm} \times 1.875 \text{ mm}$  and  $N_x \times N_y = 480 \times 480$  grid points are used. The governing equations are conservation equations of mass, momentum, energy and species concentration. In the present study, the Soret effect, the Dufour effect, pressure gradient diffusion, bulk viscosity and radiative heat transfer are assumed to be negligible.

Spatial discretization is conducted by 4th-order central finite difference scheme and the 4th-order compact finite difference filter [8] is applied to eliminate higher spatial frequency oscillations than the spatial resolution. Time integration is implemented by 3rd-order Runge-Kutta scheme except for reaction source terms. Reaction source terms in species conservation equations are advanced by the point implicit method using VODE solver [9]. Detailed kinetic mechanism including 53 species and 325 elementary reactions (GRI-Mech 3.0 [10]) for methane–air and reduced kinetic mechanism including 37 species and 61 reactions (Maroteaux and Noel [11]) for n-heptane–air mixtures are adopted. Temperature dependence of viscosity, thermal conductivity and diffusion coefficients are taken into account by linking CHEMKIN packages [12, 13] with modifications for vector/parallel computations.

### 3 Effects of Spatial Temperature Inhomogeneity on HCCI Combustion

In this section, influences of temperature fluctuations on HCCI combustion characteristics are discussed using the DNS results for methane–air mixture. Figure 1(a) shows temporal developments of the maximum, minimum and mean temperature in the computational domain. For the homogeneous case, temperature starts increasing gradually after  $t = 1000 \mu\text{s}$  and ignition delay time is  $1381 \mu\text{s}$ . Here, ignition delay time is defined by the inflection point of temporal development of temperature. For the case with  $T'_{init} = 12 \text{ K}, 60 \text{ K}, 90 \text{ K}$  and  $120 \text{ K}$ , ignition delay time is  $1377 \mu\text{s}, 1212 \mu\text{s}, 825 \mu\text{s}$  and  $411 \mu\text{s}$ , respectively. For the  $T'_{init} = 12 \text{ K}$  case, there is no large difference between the maximum and minimum temperature during thermal runaway and ignition delay time is comparable to the homogeneous case. From the case with  $T'_{init} = 12 \text{ K}$  to  $90 \text{ K}$ , time interval between the maximum and minimum temperature becomes longer.

Figure 1(b) shows temporal developments of the maximum, minimum and mean values of heat release rate normalized by the maximum heat release rate of the homogeneous case. For the homogeneous case, the heat release rate increases rapidly and decreases in a short period. For  $T'_{init} = 12 \text{ K}$ , the mean heat release rate rises rapidly similar to the homogeneous case, but the maximum value decreases to 86 % of that for the homogeneous case due to the temperature inhomogeneity. For  $T'_{init} = 60 \text{ K}, 90 \text{ K}$  and  $120 \text{ K}$  cases, mean heat release rate rises slowly and the maximum value decreases to 41 %, 25 % and 17 %

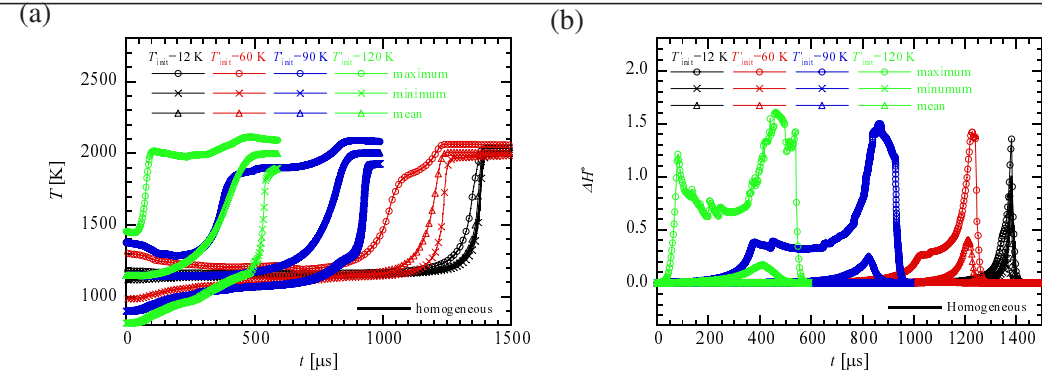


Figure 1: Temporal developments of the maximum, minimum and mean values of temperature (a) and of normalized heat release rate (b) for methane–air mixture.

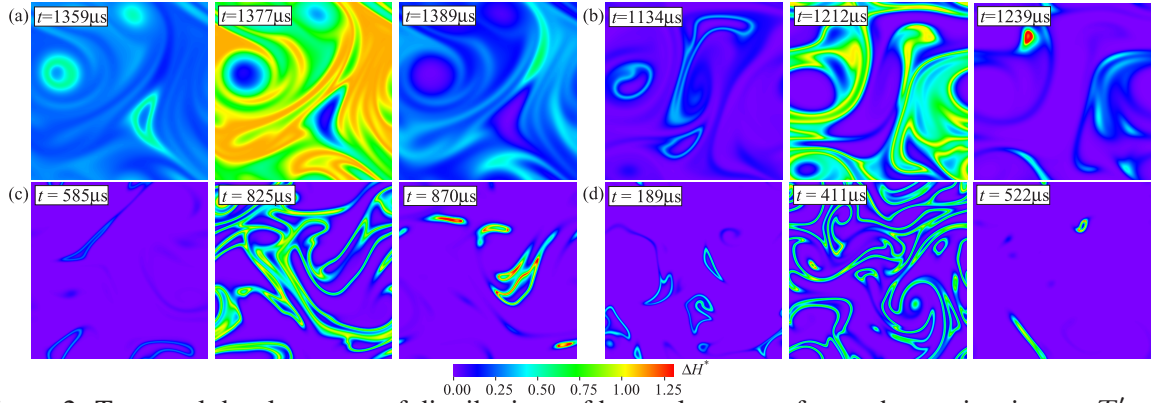


Figure 2: Temporal developments of distributions of heat release rate for methane–air mixture.  $T'_{\text{init}} = 12 \text{ K}$  (a),  $60 \text{ K}$  (b),  $90 \text{ K}$  (c),  $120 \text{ K}$  (d).

of that for the homogeneous case, respectively. Once the maximum heat release rate increases because of local autoignition, and then starts to increase again at  $400 \mu\text{s}$ ,  $750 \mu\text{s}$  and  $1150 \mu\text{s}$  for  $T'_{\text{init}} = 60 \text{ K}$ ,  $90 \text{ K}$  and  $120 \text{ K}$ , respectively. This second increase is induced by pressure increase which results in higher release rate. For  $T'_{\text{init}} = 120 \text{ K}$ , the maximum heat release rate decreases after local autoignition because ignition kernel is much smaller compared with other cases which results in rapid diffusion of heat and radicals toward low temperature unburnt region.

Initial temperature fluctuations also affect combustion manner locally. Figure 2 shows temporal developments of distributions of heat release rate normalized by the maximum heat release rate of the homogeneous case. For  $T'_{\text{init}} = 12 \text{ K}$  case, local autoignition starts from higher temperature regions and the thick flame-like structures propagate from the ignition kernels in a short period (see  $t = 1359 \mu\text{s}$  in Fig. 2(a)) and then autoignition occurs in almost whole domain. For  $T'_{\text{init}} = 60 \text{ K}$  case, after the local autoignition, flame fronts are formed ( $t = 1134 \mu\text{s}$  in Fig. 2(b)) and spread from ignition kernels ( $t = 1212 \mu\text{s}$  in Fig. 2(b)). Around the ignition delay time, autoignition occurs in the whole unburnt regions at  $t = 1212 \mu\text{s}$ . For the case with  $T'_{\text{init}} = 90 \text{ K}$  and  $120 \text{ K}$  in Fig. 2(c) and (d), thinner flames are formed after local autoignitions. Then, flame fronts propagate from ignition kernels with deformation and rotation under the influence of strain and vorticity of turbulence. For these cases, flames enclose finally and the unburnt gas is consumed rapidly. Note that autoignition does not occur after flame propagation for these cases.

#### 4 Classification of Combustion Regimes by Using Fluid Particle Tracking

Combustion characteristics significantly depend on temperature fluctuations and seem to be classified into three regimes locally: autoignition, flame propagation and rapid unburnt mixture consumption by

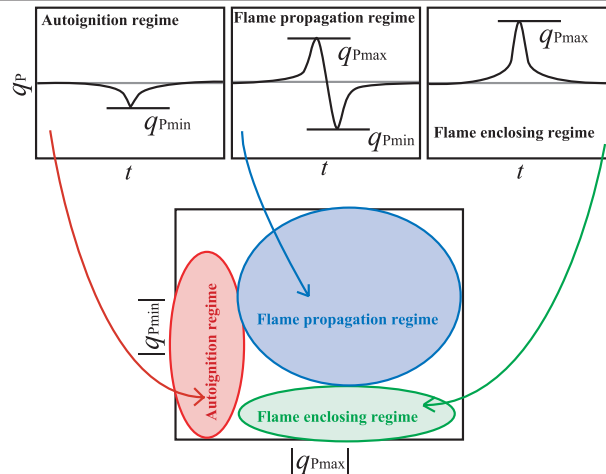


Figure 3: Combustion regime classification for autoignition, flame propagation and flame enclosing.

flame enclosure as shown in previous section. To classify combustion regimes for turbulent HCCI combustion, Lagrangian fluid particle tracking algorithm is included in the present DNS and time histories of various physical and chemical quantities on the each fluid particle are stored. Positions of particles are tracked based on the equation,  $d\mathbf{x}_P/dt = \mathbf{v}[\mathbf{x}_P(t)]$ , and 3rd-order Runge-Kutta scheme is applied for time integration. Velocity on each particle,  $\mathbf{v}[\mathbf{x}_P(t)]$ , is obtained by using 4th order Lagrangian interpolation of fluid velocity.

In this study, time history of heat conduction,  $q_P = \nabla \cdot (\lambda \nabla T)_P$  on the fluid particle, is used for the combustion regime classification. Heat conduction on the particles in autoignition regime shows a slight heat loss after autoignition since the fluid element in autoignition regime does not need heat supply for ignition due to local high temperature enough for autoignition and heat diffuses from the autoignition kernel to the surrounding unburnt gas. For the particles in propagating flame regime, heat conduction increases and then decreases since heat is transported to the fluid elements from burnt gas when flame front reaches the particles and then heat diffuses to unburnt gas after the flame passes through the particles. For the particles in flame enclosing regime, heat conduction shows gain since surrounding flame fronts supply heat to unburnt gas island.

Considering above time history of heat conduction on each fluid element, classification method of the combustion regimes is shown in Fig. 3, schematically.  $|q_{P\max}|$  and  $|q_{P\min}|$  denote the maximum and minimum heat conduction on each particle. From the absolute values  $|q_{P\max}|$  and  $|q_{P\min}|$  on these particles, the combustion regime of each fluid element are identified. Particles in autoignition regime are located in red zone in Fig. 3 where  $|q_{P\max}|$  is low. Particles in propagating flame regime are plotted in blue zone where both  $|q_{P\max}|$  and  $|q_{P\min}|$  are high. Particles in flame enclosing regime are classified into green zone where only  $|q_{P\max}|$  is high.

This classification scheme is applied for turbulent HCCI combustion. 921600 particles are tracked for turbulent cases. Figure 4(a)-(d) shows probability density functions (PDFs) of  $|q_{P\max}|$  and  $|q_{P\min}|$  for turbulent HCCI combustion of methane-air mixture. Red color in each figure shows maximum probability. A straight line shows  $|q_{P\max}| = |q_{P\min}|$ . It is noted that the ranges of  $|q_{P\max}|$  and  $|q_{P\min}|$  are different for the cases. For  $T'_{\text{init}} = 12$  K, almost all fluid elements are classified into autoignition regime. For  $T'_{\text{init}} = 60$  K, although majority of mixture is also classified into autoignition regime, there are low probability of mixture which burn in propagating flame regime due to the existence of flame fronts as shown in Fig. 2(b). For  $T'_{\text{init}} = 90$  K, one peak is found on each combustion regime. The probabilities of three kinds of combustion regimes are almost equal for this case. For  $T'_{\text{init}} = 120$  K, the probability of flame enclosing regime is highest and that of propagating flame regime is also

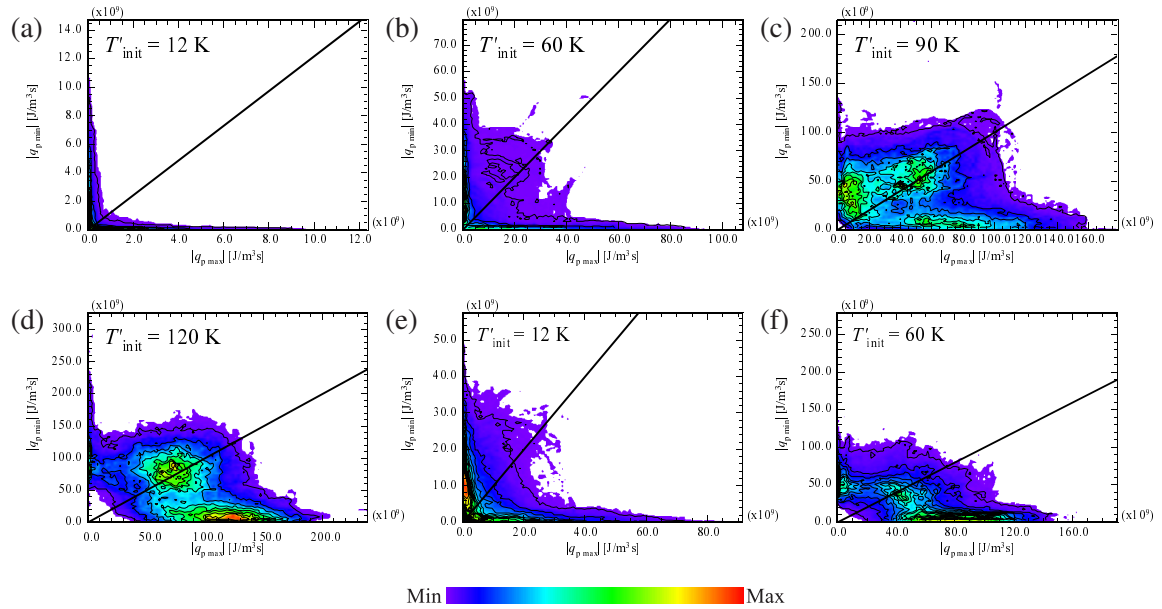


Figure 4: PDFs of  $|q_{P\max}|$  and  $|q_{P\min}|$  for turbulent HCCI combustion of methane–air mixture ((a)-(d)) and n-heptane–air mixture ((e)-(f)).

high, whereas that of autoignition is very low. These classified combustion regimes well coincide with the observation in Fig. 2. For the initial mixture condition adopted in this study, it is concluded that dominant phenomena is autoignition for  $T'_{\text{init}} \leq 60 \text{ K}$  and is flame propagation for  $T'_{\text{init}} \geq 90 \text{ K}$ . For  $T'_{\text{init}} \geq 90 \text{ K}$ , autoignition region only works as heat source for inducing flame propagation.

The same classification method is applied to the DNS results for n-heptane–air cases. In Fig. 4(e)-(f), PDFs of  $|q_{P\max}|$  and  $|q_{P\min}|$  for n-heptane–air cases are shown. For the case with  $T'_{\text{init}} = 12 \text{ K}$ , high probability is observed in autoignition regime and probability in propagating flame and flame enclosing regime is low. In this case, values of  $|q_{P\max}|$  and  $|q_{P\min}|$  are higher than the methane–air case with the same temperature fluctuations. For the case with  $T'_{\text{init}} = 60 \text{ K}$ , one peak is observed in each combustion regime and flame enclosing regime shows the highest probability. These results suggest that transition from autoignition to propagating flame and then flame enclosing regime also occurs for n-heptane–air case at lower initial temperature fluctuations and that effects of temperature fluctuations on combustion characteristics are larger for n-heptane–air mixtures compared to the methane–air mixtures.

## 5 Summary

In the present study, DNS studies on autoignition of methane–air and n-heptane–air mixtures have been conducted by considering realistic kinetic mechanism and temperature dependence of transport and thermal properties. Combustion process strongly depends on temperature fluctuations. Combustion regime classification method using Lagrangian fluid particle tracking is proposed. This method is based on the fact that heat conduction on each fluid element shows different characteristics in the three combustion regimes, autoignition regime, flame propagation regime and flame enclosing regime. The dominant consumption process transits from autoignition to flame propagation and then to flame enclosing regime with increasing in initial temperature fluctuations. These transitions are observed for different fuels: methane and n-heptane. For the combustion conditions investigated in the present study, the transition from autoignition to flame propagation occurs at  $T'_{\text{init}} \approx 90 \text{ K}$  for methane and at  $T'_{\text{init}} \approx 60 \text{ K}$  for n-heptane.

## Acknowledgment

This research is partially granted by the Japan Society for the Promotion of Science through the “Funding Program for Next Generation World-Leading Researchers (NEXT program) ” (No. GR038) initiated by the Council for Science and Technology Policy.

## References

- [1] K. Epping, S. Aceves, R. Bechtold, J. Dec. (2002). The Potential of HCCI Combustion for High Efficiency and Low Emissions. SAE Technical Paper, Paper No. 2002-01-1923.
- [2] Echekki, T., and J.H. Chen. (2003). Direct Numerical Simulation of Autoignition in Non-Homogeneous Hydrogen–Air Mixtures. *Combust. Flame* 134 (3): 169-191.
- [3] E.R. Hawkes, R. Sankaran, P.P. Pébay, J.H. Chen. (2006). Direct Numerical Simulation of Ignition Front Propagation in a Constant Volume with Temperature Inhomogeneities; II. Parametric Study. *Combust. Flame* 145 (1-2): 145-159.
- [4] C.S. Yoo, T. Lu, J.H. Chen, C.K. Law. (2011). Direct Numerical Simulations of Ignition of a Lean n-Heptane/Air Mixture with Temperature Inhomogeneities at Constant Volume: Parametric study. *Combust. Flame* 158 (9): 1727-1741.
- [5] J.H. Chen, E.R. Hawkes, R. Sankaran, S.D. Mason, H.G. Im. (2006). Direct Numerical Simulation of Ignition Front Propagation in a Constant Volume with Temperature Inhomogeneities; I. Fundamental Analysis and Diagnostics. *Combust. Flame* 145 (1-2): 128-144.
- [6] D.J. Cook, H. Pitch, J.H. Chen, E.R. Hawkes. (2007). Flamelet-based Modeling of Auto-Ignition with Thermal Inhomogeneities for Application to HCCI Engines. *Proc. Combust. Inst.* 31: 2903-2911.
- [7] Y. Ju, W. Sun, M.P. Burke, X. Gou, Z. Chen. (2011) Multi-Timescale Modeling of Ignition and Flame Regimes of n-Heptane-Air Mixtures near Spark Assisted Homogeneous Charge Compression Ignition Conditions. *Combust. Flame* 158 (1): 1727-1741.
- [8] S.K. Lele. (1992). Compact Finite Difference Schemes with Spectral-Like Resolution. *J. Comput. Phys.* 103: 16-42.
- [9] P.N. Brown, G.D. Byrne, A.C. Hindmarsh. (1989). VODE, a Variable-Coefficient ODE Solver. *SIAM J. Sci. Stat. Comp.* 10: 1038-1051.
- [10] C.T. Bowman, R.K. Hanson, D.F. Davidson, W.C. Gardiner Jr, V. Lissianski, G.P. Smith, D.M. Golden, M. Frenklach, M. Goldenberg. Available from [http://www.me.berkeley.edu/gri\\_mech](http://www.me.berkeley.edu/gri_mech)
- [11] F. Maroteaux, L. Noel. Development of a Reduced n-Heptane Oxidation Mechanism for HCCI Combustion Modeling. *Combust. Flame* 146 (1-2): 246-267.
- [12] R.J. Kee, G. Dixon-Lewis, J. Warnatz, M.E. Coltrin, J.A. Miller. (1986). A Fortran Computer Code Package for the Evaluation of Gas-Phase Multicomponent Transport Properties. Sandia Report, Report No. SAND86-8246.
- [13] R.J. Kee, F.M. Rupley, J.A. Miller. (1989). Chemkin-II: A Fortran Chemical Kinetics Package for the Analysis of Gas Phase Chemical Kinetics. Sandia Report, Report No. SAND89-8009B